Rupture process of the 2007 Niigata-ken Chuetsu-oki earthquake by non-linear joint inversion of strong motion and GPS data

Cirella, A., A. Piatanesi, E. Tinti and M. Cocco

Istituto Nazionale di Geofisica e Vulcanologia
Via di Vigna Murata 605, 00143 Roma, Italy
(cirella@ingv.it, piatanesi@ingv.it, tinti@ingv.it, cocco@ingv.it)

Draft for submittal to the GRL
2008

Abstract

We image the rupture history of the 2007 Niigata-ken Chuestu-oki (Japan) earthquake by a nonlinear joint inversion of strong motion and GPS data, retrieving peak slip velocity, rupture time, rise time and slip direction. The inferred rupture model contains two asperities; a small patch near the nucleation and a larger one located 10÷15 km to the south-west. The maximum slip ranges between 2.0 and 2.5 m and the total seismic moment is 1.6×10^{19} Nm. The inferred rupture history is characterized by rupture acceleration and directivity effects, which are stable features of the inverted models. These features as well as the source-to-receiver geometry are discussed to interpret the high peak ground motions observed (PGA is 1200 gals) at the Kashiwazaki-Kariwa nuclear power plant (KKNPP), situated on the hanging-wall of the causative fault. Despite the evident source effects, predicted PGV underestimates the observed values at KKNPP by nearly a factor of 10.

1. Introduction

The 2007 Niigata-ken Chuestu-oki earthquake (M_w 6.6) occurred near the west coast of Honshu, Japan, on July 16th at 01:13 UTC (Figure 1). The epicenter has been located at 37.557°N, 138.608°E (Japan Meteorological Agency). This earthquake caused severe damages and fatalities around the source region. In particular, the earthquake struck the Kashiwazaki-Kariwa nuclear power plant (KKNPP), placed on the hanging wall of the causative fault, where a peak ground acceleration (PGA) associated with surface motions exceeding 1200 gals has been recorded (Irikura *et al.*, 2007). The 2007 Niigata-ken Chuetsu-oki earthquake is one of the few large events whose causative fault extends beneath a nuclear power plant; for this reason it attracts the attention of both the geophysical and engineering communities. Moreover, this region was previously struck by another severe earthquake, the 2004 Mid Niigata Prefecture earthquake (M_w = 6.6), occurred 50 km to the southeast of the hypocenter of the 2007 earthquake. Because of the impact of these earthquakes and the associated hazard, the understanding of their source and rupture history is extremely important.

The Niigata-Kobe Tectonic Zone (NKTZ) is characterized by a compressional regime due to the convergence of the Amur plate and the Okhotsk plate. This high strain-rate zone is characterized by shortening tectonics with E-W- to NW-SE trending compressive axis (Nakajima and Hasegawa, 2007). Consistently, the focal mechanism of the 2007 Niigata-ken Chuetsu-oki earthquake, estimated by the moment tensor analysis (F-net: http://www.fnet.bosai.go.jp), shows reverse faulting with conjugate nodal planes dipping to NW and SE (plane 1: N215°E, 49°, 80°; plane 2: N49°E, 42°, 101° for strike dip and rake angle, respectively). The identification of rupture plane of the 2007 Niigata-ken Chuetsu-oki earthquake has been debated in the literature. Aoi *et al.* (2007) adopted both nodal planes as candidate faults for their waveform inversion approach. These authors point out that a similar fit to the recorded data can be achieved using the two nodal planes as the rupture planes. However, the spatial distribution of relocated aftershocks (e.g., DPRI, 2007: http://www.eqh.dpri.kyoto-ac.jp/~mori/niigata/reloc.html) displays a fairly clear eastward dipping plane. Furthermore, recent studies (Toda, 2007; Koketsu *et al.*, 2007) of the 2007 Niigata-ken Chuetsu-oki earthquake, propose the SE dipping nodal plane as the preferred fault plane. Finally, Irikura *et al.* (2007) identify the same fault plane by analyzing the aftershocks relocated using data from ocean bottom seismometers.

The dense strong motion seismic networks KiK-net (http://www.kik.bosai.go.jp) and K-NET (http://www.k-net.bosai.go.jp) allowed us to collect a large number of ground motion records. Data from several continuous GPS stations deployed by the Geographical Survey Institute (GSI) are also available. In this study, we investigate the rupture process of the 2007 Niigata-ken Chuetsu-oki earthquake, by jointly inverting strong-motion seismic data and GPS measurements. The goal is to constrain the rupture history to better understand the mechanics of the causative fault as well as the observed ground shaking at the nuclear power plant.

2. Inversion methodology

In order to retrieve the rupture history of the 2007 Niigata-ken Chuetsu-oki earthquake, we use a two-stage nonlinear inversion method (Piatanesi *et al.* 2007); this technique is able to jointly invert strong ground motions records and geodetic data. The extended fault is divided into subfaults with model parameters assigned at the corners; the value of every parameter is not constant inside the subfault but it spatially varies through a bilinear interpolation of the nodal values. At each point on the fault the rupture model is described by four model parameters: rise time, rupture time, peak slip velocity and rake angle. Each point on the fault can slip only once (single window approach) and the source time function can be selected among different analytical forms (e.g. box-car, triangular, exponential, regularized Yoffe) implemented in the adopted procedure (Cirella *et al.*, 2007). In this study, we assume a regularized Yoffe function (Tinti *et al.*, 2005) with T_{acc} (time of peak slip velocity) equal to 0.3 sec, this choice being compatible with dynamic earthquake modeling (e.g., Mikumo et al., 2003). The final slip distribution is derived by the inverted parameters and depends on the choice of the source time function and T_{acc}.

The nonlinear global inversion consists of two stages. In the first stage an heat-bath simulated annealing algorithm builds up the model ensemble. The algorithm starts its search by a random model and then it perturbs the model parameters one by one. Then, for each possible configuration, the forward modeling is performed with a Discrete Wave-Number technique (Spudich and Xu, 2003), whose Green's function includes the complete response of the 1-D Earth structure. Observed and predicted data are compared in the frequency domain. For strong motion data we use an objective cost function that is an hybrid representation between L1 and L2 norms, while the cost function related to the GPS measurements is a sum-squared of the residuals between synthetic and recorded static displacements normalized to the observed data (equations (2) and (3) in Piatanesi *et al*., 2007). The total cost function is computed from the summation of the weighted cost functions of the two datasets. After testing the best weights' combinations with trial and error runs, in this application we have decided to adopt the same weights for the two different datasets.

In order to make the model ensemble independent of a particular choice of the initial model, the algorithm is conceived to perform multiple restarts with different random models. During the first stage, all models and their cost function values are saved to build up the model ensemble. In the second stage the algorithm performs a statistical analysis of the ensemble providing us the best-fitting model, the average model and the associated standard deviation (see eq.(5) and eq.(6) in Piatanesi *et al*., 2007) computed by weighting all models of the ensemble by the inverse of their cost function values. These estimates represent the ensemble properties and are the actual solution of our nonlinear inverse problem. This approach allows us to extract the most stable features of the rupture process that are consistent with the data as well as to assess model uncertainties.

3. Rupture Process of the 2007 Niigata-ken Chuetsu-oki Earthquake

3.1 Data and fault model

Strong motion data from 13 stations of KiK-net and K-NET and 14 GPS records of the co-seismic surface displacement (GSI) are used in our modeling attempts. Their focal distances are less than 70 km and their locations are displayed in Figure 1. We have also plotted in this figure the location of two GPS benchmarks (960566, 960567) and one accelerograph (NIG018) that are not used in the inversion presented in this study. These GPS data have been excluded because the instrumentation and/or the corrected coseismic displacements might have problems (S. Aoi and K. Koketsu, personal communication**s**).

Moreover, we have not used the waveforms recorded at the NIG018 site, which is the closest to the KKNPP power plant, because it is strongly affected by non-linear site effects. However, we have verified that including or excluding these data does not change the inverted source model.

Original acceleration recordings are integrated to obtain ground velocity time histories. The resulting velocity waveforms are band-pass filtered between 0.02 and 0.5 Hz using a two-pole and two-pass Butterworth filter. We invert 60 seconds of each waveform, including body and surface waves. Despite the high number of triggered stations, the azimuthal coverage is limited to ~180° due to the off-shore location of the epicenter (Figure 1). However, the results of a synthetic test (see auxiliary material) reveal that the station distribution is good enough to image model parameters.

The hypocenter location by H-net data is 37.54°N, 138.61°E with 8.9 km depth (Yukutake *et al.*, 2007). We perform the inversion assuming a rupture starting point at the hypocenter located at 8 km depth and on the south-east dipping fault (Figure 1), striking N49°E and dipping 42° (F-net solution). According to aftershocks distribution we assume a fault model with a length of 38.5 km and a width of 31.5 km; the top of the fault is located at 0.5 km depth. All kinematic parameters are simultaneously inverted at nodal points every 3.5 km equally spaced along strike and dip. During the inversion, the peak slip velocity is allowed to vary between 0 and 4 m/s with 0.25 m/s step increment and the rise time between 1 and 4 sec with 0.25 step increment. The rake angle ranges between 71° and 131° with 5° step increment (the rake angle of the moment tensor solution of F-net is 101°); the rupture time distribution is constrained by a rupture velocity ranging between 2 and 4 km/s. To calculate the Green’s functions, we adopt a 1D- crustal model referring to the velocity structure proposed by Kato *et al.* (2005).

3.2 Inversion results

The adopted algorithm explores about 2 millions rupture models to build up the model ensemble. Figure 2-a shows the inverted source model obtained by averaging a subset of the model ensemble (nearly 300.000 rupture models), corresponding to those models having a cost function exceeding by 2.5% the minimum value of the cost function reached during the inversion. Left panel in Figure 2-a displays the final slip distribution, middle and right panels show the rise time and the peak slip velocity distributions on the fault plane, respectively. The left panel also shows the slip direction at each grid node. The retrieved model is characterized by two principal patches of slip: a small patch near the nucleation point and a larger one located at 10÷15 km south-west from the nucleation. The larger asperity is characterized by a rise time ranging between 2.5 and 3.5 sec and a peak slip velocity of 2.0÷3.5 m/s, corresponding to 1.5÷2.5 m of slip. The inferred slip distribution and the resulting seismic moment ($M_0 = 1.6 \times 10^{19}$ Nm) fairly agree with those inferred by Aoi *et al.* (2007).

The slip direction, shown in the left panel of Figure 2-a (black arrows), is consistent with a nearly pure reverse faulting mechanism. The total rupture duration is about 10 sec. In correspondence of the larger asperity, the rupture front rapidly accelerates from 2.3 km/s to 3.5 km/s. The rupture acceleration occurs in the south-western portion of the fault plane, very close to KKNPP.

The adopted inversion methodology has the advantage to provide both the best fitting and the average source models with the corresponding standard deviations of model parameters. Figure 2-b shows the standard deviations of rupture time, rise time and peak slip velocity. We point out that the imaged acceleration of the rupture front is a stable feature and it is associated with relatively small standard deviations. As expected, standard deviations of rise time are larger in the areas of small or negligible slip. Moreover, the absolute values of peak slip velocity display a larger variability in the high slip patches. The retrieved best fitting model displays main features similar to the average one.

We show in Figure 2-c-d the fit to the observed data. The simulated time histories match fairly well the recorded data at most of the stations (Figure 2-c). Discrepancies at some sites can be due to the complex wave propagation in a heterogeneous medium as well as to the surface waves generated in shallow sedimentary layers not simulated in our modeling. By checking the shallow velocity structure below the recording sites, we have verified that the poor match between horizontal components of recorded and predicted waveforms at NIG013 is likely due to site amplification effects. Moreover, the fit between synthetic and observed coseismic horizontal displacement vectors at the selected GPS stations shows a good agreement (Figure 2-d). Indeed, the coseismic deformation pattern is consistent with dip slip motion, as resulting by the inferred distribution of slip direction. We have also computed and plotted in this figure the predicted displacement at the 960567 site (indicated by the dashed line), because it is close to KKNPP.

4. Discussion and Conclusive remarks

The main goal of this study is to image the rupture history during the 2007 Niigata-ken Chuetsu-oki earthquake by inverting available geodetic and strong motion data. However, the most peculiar feature of this earthquake is the presence of a nuclear power plant in the hanging wall of the causative fault. The inferred source model is characterized by a non-uniform slip distribution and a heterogeneous rupture propagation. Slip velocity is concentrated in two patches relatively close to the nuclear power plant (KKNPP), with a slip velocity peak of nearly (3.50 ± 0.75) m/s. The maximum observed PGA, among the accelerograms available to the authors, is 813 cm/s^2 recorded at K-NET Kashiwazaki station (NIG018), which is the closest site to KKNPP. Although the proposed model is able to fit most of the available data, it is not able to reproduce the observed amplitudes at the NIG018 site.

In order to quantitatively assess the source contribution to the ground shaking observed at the nuclear power plant, we have performed a forward estimate of predicted ground motions. By using the inverted rupture model, we have simulated ground velocity time histories at a virtual dense array of seismic stations (889 sites, see Figure 3-a), 14 of which correspond to the actual recording sites mapped in Figure 1. In this way we get a good azimuthal coverage and a dense sampling of the near source area. Figure 3 shows the distributions of the simulated PGV values for the fault-parallel, fault-normal and vertical components. PGV is measured from synthetic seismograms filtered in the same frequency bandwidth adopted for waveform inversion.

The pattern of peak ground velocity reflects the fault geometry, the heterogeneous slip distribution and rupture SW acceleration, revealing clear directivity effects. The high values of PGV predicted southwestward of the hypocenter are mostly due to the slip distribution and source-to-receiver geometry. Despite this relevant rupture directivity effect, the predicted PGV at NIG018 underestimates the observed value (filtered in the same frequency bandwidth as synthetics) by nearly a factor 10. This result confirms that other effects associated with complex propagation paths and site amplifications contributed to explain the severe ground motion recorded at KKNPP. Worthy of note is the observation that recorded PGA at KKNPP is much larger (nearly two times) than the adopted design value (Sugiyama, 2007).

We emphasize that the average rupture model proposed in this study by inverting GPS and strong motion data includes the most relevant features of roughly 300.000 models, which yield a reasonable fit to the observed data. In particular, the adopted inversion procedure allows us to analyze the standard deviations of model parameters and to conclude that the rupture acceleration as well as the directivity effects are stable features of the causative earthquake rupture. We believe that this approach is of relevance to constrain the variability of kinematic model parameters, and it represents an important step towards the performing of reliable predictions of ground motion time histories.

Acknowledgments. The authors are grateful to Shin Aoi and Kazuki Koketsu for the information. Thanks to K-NET and KiK-net for providing strong motion data, and to GSI for providing GPS data. Some figures are made using Generic Mapping Tools free software (*Wessel and Smith*, 1998). We thank two anonymous referees and the editor for their useful comments.

References

Aoi, S., H. Sekiguchi, N. Morikawa, T. Ozawa, T. Kunugi, M. Shirasaka (2007), Source Process of the 2007 Niigata-ken Chuetsu-oki Earthquake derived from Near-fault Strong Motion Data, *Eos Trans. AGU, 88*(52), Fall Meet. Suppl., Abstract S54A-04.

Cirella, A., A. Piatanesi, P. Spudich, M. Cocco and E. Tinti (2007), Using a Global Search Inversion to Constrain Earthquake Kinematic Rupture History and to Assess Model Uncertainty, *Eos Trans. AGU, 88*(52), Fall Meet. Suppl., Abstract S53C-03.

Irikura, K., T. Kagawa, K. Miyakoshi, S. Kurahashi (2007), Rupture process and strong ground motions of the 2007 Niigataken Chuetsu-Oki earthquake – Directivity pulses striking the Kashiwazaki-Kariwa Nuclear Power Plant-, *Eos Trans. AGU, 88*(52), Fall Meet. Suppl., Abstract S31B-0441.

Kato, A., E. Kurashimo, N. Hirata, S. Sakai, T. Iwasaki and T. Kanazawa (2005), Imaging the source region of the 2004 mid-Niigata prefecture earthquake and the evolution of a seismogenic thrust-related fold, *Geophys. Res. Lett*., 32, L07307, doi:10.1029/2005GL022366.

Koketsu, K., H. Miyake, K. Hikima (2007), Source Inversion for the 2007 Chuetsu-oki, Japan, Earthquake: A Case of Difficulty Determining the Source Fault Plane, *Eos Trans. AGU, 88*(52), Fall Meet. Suppl., Abstract S54A-05.

Mikumo, T., K. B. Olsen, E. Fukuyama, and Y. Yagi (2002). Stress-breakdown time and slip-weakening distance inferred from slip-velocity functions on earthquake faults, *Bull. Seism. Soc. Am.*, 93(1), 264–282.

Nakajima, J. and A. Hasegawa (2007), Deep crustal structure along the Niigata-Kobe Tectonic Zone, Japan: Its origin and segmentation, *Earth Planets Space,* 59, e5-e8.

Piatanesi, A., A. Cirella, P. Spudich, and M. Cocco (2007), A global search inversion for earthquake kinematic rupture history: Application to the 2000 western Tottori, Japan earthquake, *J. Geophys. Res.,* 112, B07314.

Spudich, P. and L. Xu (2003), Software for calculating earthquake ground motions from finite faults in vertically varying media, in *International Handbook of Earthquake and Engineering Seismology*, Academic Press.

Sugiyama, Y (2007), 16 July 2007 Niigata-ken Chuetsu-oki earthquake; its characteristics, tectonic background and significance for active fault evaluation, *Eos Trans. AGU, 88*(52), Fall Meet. Suppl., Abstract T31G-01.

Tinti, E., E. Fukuyama, A. Piatanesi and M. Cocco (2005), A kinematic source time function compatible with earthquake dynamics, *Bull. Seismol. Soc. Am.*, 95(4), 1211-1223, doi:10.1785/0120040177.

Toda, S. (2007), 2007 Mw=6.6 Niigata Chuetsu-Oki earthquake ruptured on a fault strongly unclamped by the 2004 Mw=6.6 Niigata Chuetsu shock, *Eos Trans. AGU, 88*(52), Fall Meet. Suppl., Abstract S13B-1301.

Wessel, P. and W.H.F. Smith (1998), New, improved version of the Generic Mapping Tools released, *EOS Trans. AGU,* 79, 579.

Yukutake, Y., T. Takeda, and K.Obara (2007), Spatial distribution of aftershocks in the region of Niigata Tyuetsu-oki Earthquake in 2007, by waveform correlation analysis, *Seismol. Soc. Jpn. Programme. Abstr. Fall Meeting*, PI-063, (in Japanese).

Figure captions

Figure 1. Map of the fault geometry of the 2007 Niigata-ken Chuestu-oki, Japan earthquake. The dashed black line represents the surface projection of the fault plane adopted in this study. Black star indicates the epicenter. White triangles and inverted triangles represent K-NET (surface sensor) and KiK-net (borehole sensor) strong motion stations respectively. Black dots represent GPS stations. White dots are GPS stations not used in this study. KKNPP indicates the site of Kashiwazaki-Kariwa nuclear power plant.

Figure 2. a) Inverted rupture model (average model from ensemble inference) of the 2007 Niigata-ken Chuestu-oki earthquake. Left, middle and right panels show total slip, rise time and peak slip velocity distributions, respectively. White color in middle panel represents the areas of small or negligible slip. Rupture time shown by contour lines (in seconds); black arrows displayed in left panel represent the slip vector. b) Standard deviation of rupture time, rise time and peak slip velocity for the average rupture model computed through ensemble inference. c) Comparison of recorded strong motions (blue lines) with predicted waveforms computed from the inverted rupture model of Figure 2-a (red lines). Numbers with each trace are peak amplitude of the synthetic waveforms in cm/s. d) Comparison of observed (blue arrows) with synthetic (red arrows) horizontal GPS displacements.

Figure 3. Predicted PGV distribution for the inverted model shown in Figure 2-a. Maps a), b) and c) display the parallel to strike, normal to strike and vertical component, respectively. White circles in panel a) indicate the grid of sites and the white label shows the location of the Kashiwazaki Kariwa nuclear power plant (KKNPP).

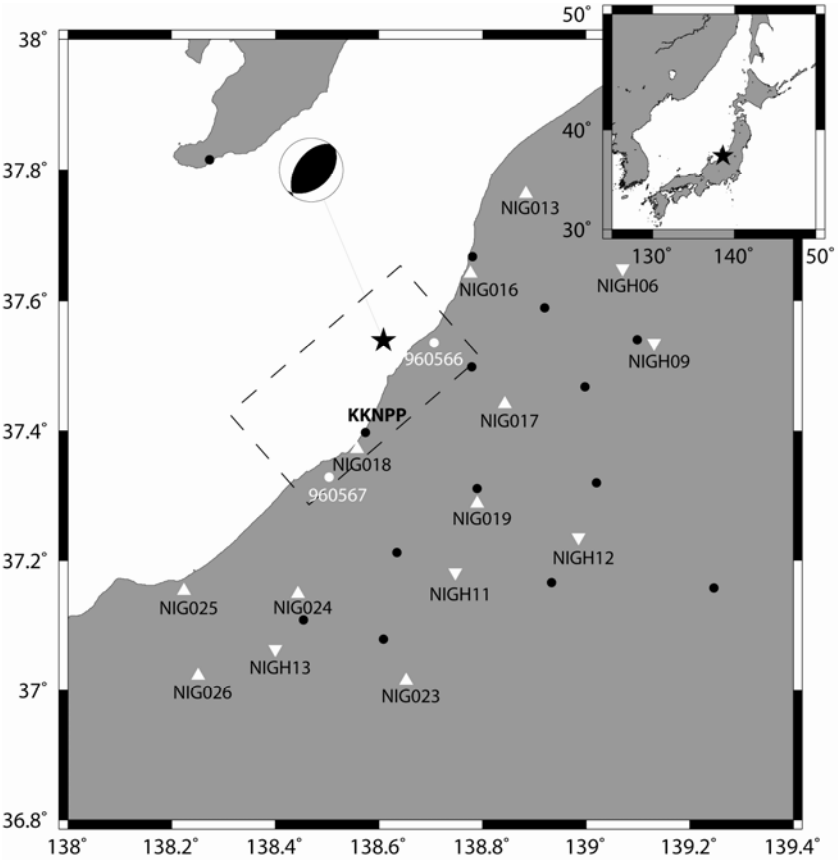
38°
37.8°
37.6°
37.4°
37.2°
37°
36.8°
138°
138.2°
138.4°
138.6°
138.8°
139°
139.2°
139.4°
50°
40°
30°
130°
140°
50°
NIG013
NIG016
NIGH06
960566
NIGH09
KKNPP
NIG017
NIG018
960567
NIG019
NIGH12
NIGH11
NIG025
NIG024
NIGH13
NIG026
NIG023

Figure1

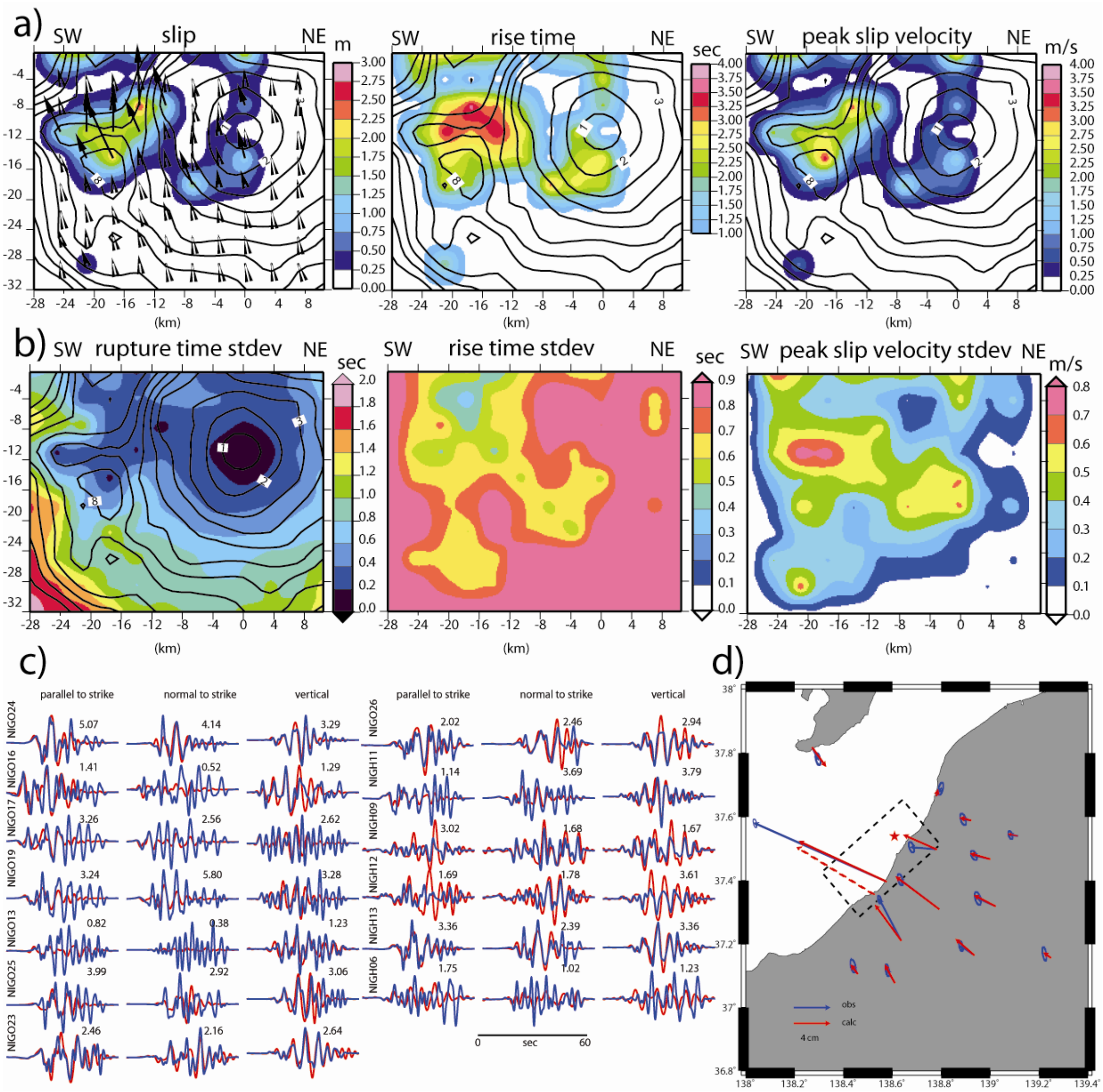

Figure2

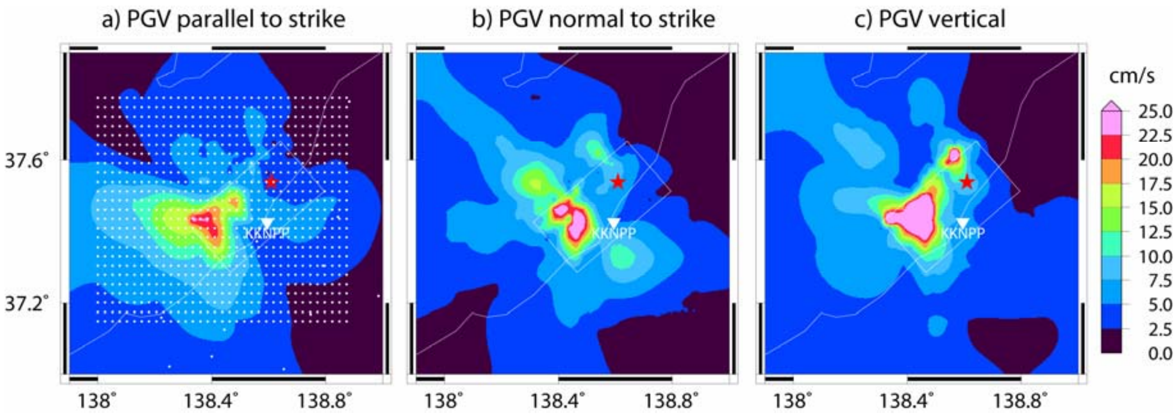

Figure3